The creep properties of Sn-12wt%Bi and Sn-12wt.%Bi-1wt%Sb alloys during phase transformation

R.H. Nada[1], F. Abd El-Salam[1], M.M. Mostafa[1], A.M.Abd El Khalek*[1,2] and H.S Mohammed[1]

1. Physics Department, Faculty of Education, Ain Shams University, Cairo, Egypt
2. Physics Department, Faculty of Science, University of Tabuk, Tabuk, Saudi Arabia

Asaad_abdelkahlk@yahoo.com, Telephone no. 00966593554325

Abstract— The variations in the steady state creep parameters observed in Sn-12wt.%Bi (alloy A) and Sn-12wt.%Bi-1wt.%Sb (alloy B) due to the annealing temperature and Sb addition in the working temperature range 333 - 413K with 10 K steps, under constant stresses 32, 35 and 39 MPa have studied with a transition point at 353K for the both alloys. The strain rate sensitivity parameter, m, and the activation volume, V, increased with increasing the working temperature to 353K. The obtained activation energies are 59.99 and 66.16 kJ/mole before transformation and 72.45 and 78.03 kJ/mole after transformation for alloys A and B respectively, characterizing the grain boundary sliding (G.B.S.) with partially diffusion before transition temperature region, and the dominant cross slipping mechanism after transition region.

Index Terms— Steady state creep; Stress; Activation energy; Strain rate; Activation volume; transition temperature; phase transformation.

1 INTRODUCTION

Tin bismuth solder alloys, which outperform the Sn-Pb alloys [1] to avoid their toxicity are extensively used in the industry. Tin is a soft material that does not work-harden permanently. Tin and its alloys may be separated into four general categories [2]: Plain alloys, solders, Babbitt, and special applications.

The Sn-57 wt.%Bi binary eutectic solder alloys is known as a useful low-temperature solder (melting at 139 ^{o}C) and has been used for more than 20 years in assembling mainframes[3].

The microstructure of the eutectic Sn-Bi alloy shows equilibrium phases of Bi and Sn with about 4% Bi in solid solution [4], since Sn has a very low solubility in Bi at eutectic temperature. When the alloy is cooled down from elevated temperature, Bi precipitates in the Sn phase [5]. Between 20 and 60 ^{o}C, shear strength of eutectic Sn-Bi (25- 50 MPa) is comparable to the eutectic of Sn-Pb. At 100 ^{0}C, eutectic Sn- Bi is much weaker and its elongation is more sensitive (i.e its elongation decreases more rapidly with increasing strain rate) than Sn-Pb [6].

Steady state creep of Sn-1wt.%Bi, Sn-2wt.%Bi and Sn-5wt.%Bi as a function of stress and temperature were studied by Milten et. al [7,8] who suggested empirical equation to show the linear dependence at low strain rate and an exponential stress dependence at higher strain rate. Their observations suggested that, dislocation climb was the active mechanism in the nonlinear region. They also found that the stress sensitivity of the steady state was similar to that of pure "Sn" and the addition of "Bi" had decreased the steady-state creep rates.

The behaviour of both transient and steady state creep of Sn-3 wt% Bi alloy was investigated [9] using constant stress ranging from 13.24 to 16.30 MPa in the aging temperatures from 300 to 683K. The observed results indicated a transition in the creep behavior occurs at a testing temperature ~330 K, where the steady state creep rate, ε_{st}, increases slowly with the testing temperature up to 330K, above which it markedly increased. This was explained by dislocation motion across the precipitate where the redistribution and coarsening of Bi-rich particles caused a gradual increase in both the transient creep parameters β and n in the low temperature range (300–320 K). The rapid increase of these parameters in the high temperature range (330–370 K) was attributed to the dissolution of Bi-rich particles and the homogenization of the alloy. The activation energy of the transient creep amounted to 19 and 31 kJ/mol before and after the transition temperature, suggest both the glide of dislocations and cross-slipping dislocation mechanisms, respectively. The activation energies of the steady state creep in the vicinity of the transition temperature and above it were found to be 39 and 48 kJ/mol pointing to a grain boundary sliding mechanism[9].

F. Abd El-Salam, et. al[1] studied the strain–time relations of Sn–7 wt.% Bi and Sn–7 wt.% Bi–1 wt.% Ag alloys under different constant stresses (8.7–19.1 MPa) in the temperature range (313–373 K). The results show that the transient and the steady state creep parameters n, β and $\dot{\varepsilon}_{st}$ depend on both the deformation temperature and the applied stress. The temperature dependence of these parameters showed a transition temperature at 343 K. The Ag-free samples were harder than those with Ag addition and this was rendered the precipitation of Bi atoms which segregate to form a non-coherent cubic α-phase in Sn–7wt.% Bi samples, while, Ag addition prevents segregation of precipitates on the grain boundaries. The analysis of the X-ray diffraction patterns showed that, Ag addition

has significantly increased the Sn crystallite size and decreases Bi crystallite size.

The aim of the present work is to study the effect of the applied stress and the Sb addition as well as the phase transformation on the creep characteristics of Sn-12wt.% Bi base alloy at working temperature range 333-413 K.

2 EXPERIMENTAL PROCEDURE

Two Tin base alloys, binary alloy (Sn–12wt.%Bi) (alloy A) and tertiary alloy (Sn–12wt.% Bi-1wt.%Sb) (alloy B) were formed from starting materials with purity 99.99% by applying the normal casting technique.

The investigated alloys were prepared by weighting the proper ratios of their constituents and melted in graphite crucible placed in an electric furnace at 623 K, (the temperature above the melting point of Sn). After melting the furnace was cooled down to room temperature. As- prepared the ingot was annealed at 463 K, to homogenize it at temperature just below the melting point, for 24h. The ingots were then swaged into wire of diameter ≈ 0.07 cm. All the specimens were then initially annealed for 2h, at 443 K (at which Sn –12wt.% Bi alloy will be in the solid solution region) and the samples (each alloy) were annealed again for 2h at 443K to eliminate the cold work introduced during swaging. The samples of each alloy were slowly cooled to room temperature with a cooling rate of $1.2\text{x}10^{-2}$ K/s to obtain mixed double ($\alpha + \beta$) phases.

The strain–time experiments were carried out using a conventional type tensile testing machine described elsewhere [1]. Isothermal strain–time experiments were performed under the constant applied stresses 32, 35 and 39 MPa at working temperatures range 333- 413 K, in steps of 10 K. The elongation in the wires was measured using a dial gauge with accuracy to 0.0 1 mm.

The structure variations were traced through the analysis of X-rays diffraction patterns. Considering that the used X-rays diffractometer is accurately calibrated, the diffracted rays breadth B is therefore, affected by the breadth B_η due to the crystallite size η, which is obtained from the full width at half maximum intensity FWHM in radians, and B_ε due to lattice strain ε. On the assumption that the particle size and the macro-strain obey a Cauchy distribution [10] as the relation:

$$(\beta\cos\theta)/\lambda = 1/\eta + (2\varepsilon\sin\theta)/\lambda \qquad (1)$$

where θ is the peak angle and λ (1.542A°) is the wavelength of the X-rays used. From the linear relation drawn between (β cos θ)/λ and (sinθ/λ), a half of the slope refers to the lattice strain ε, and the inverse number of the intercept of the axis of ordinates (y- axis) refers to the average crystallite size η, respectively.

3 EXPERIMENTAL RESULTS

Tensile creep curves carried out under the constant applied stresses 32, 35 and 39 MPa at temperatures ranging from 333 to 413 K, in steps o f 10 K for alloys A and B. The temperature dependence of the steady state creep rate $\dot{\varepsilon}_{st}$, calculated from the slopes of the linear parts of the creep curves are shown in Fig.1 (a and b) for the alloys A and B.

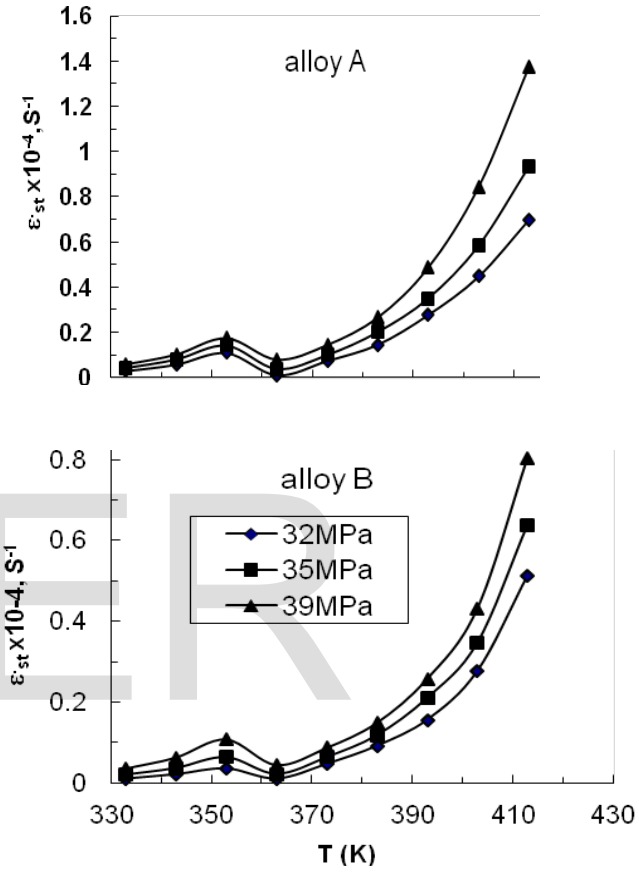

Fig. (1): The steady state strain rate ($\dot{\varepsilon}_{st}$) as a function of working temperature for both alloys A and B.

In Fig. 1 (a and b) with increasing the working temperature and/or the applied stress, $\dot{\varepsilon}_{st}$ increase slowly in the low working temperature range 333–353 K exhibiting minimum values at 363K, above which a rapid increase occurs starting from 373 K in both alloys. From the slope of the linear stress dependence ($\dot{\varepsilon}_{st}$), the strain rate sensitivity parameter, m, which is related to the stress exponent n, as 1/m [11] is calculated using the empirical equation,

$$m = \partial(\ln\sigma)/\partial(\ln\dot{\varepsilon}_{st}) \qquad (2)$$

The temperature dependence of the strain rate sensitivity parameter, m, is shown in Fig.2. From the figure the values of m at the transition temperature 353K are 0.426 and, 0.182 for both alloys A and B, respectively. Figure 3 (a and b) shows the relation between, $\ln\dot{\varepsilon}_{st}$ and σ at different working temperatures, T, for alloys A and B.

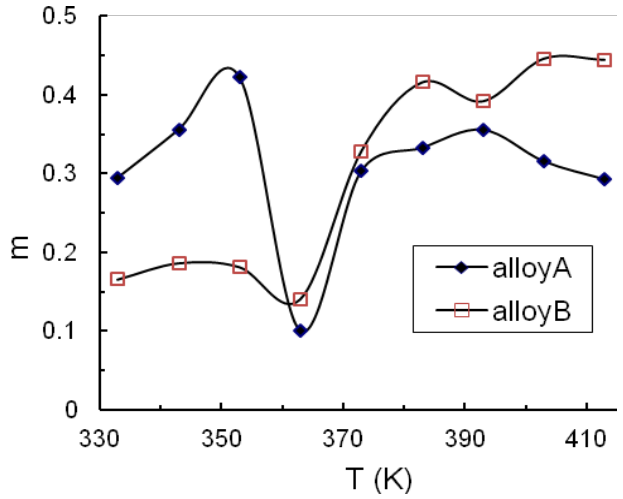

Fig.(2):The dependence of the strain rate sensitivity parameter, m, on the working temperature, T, for both alloys A and B.

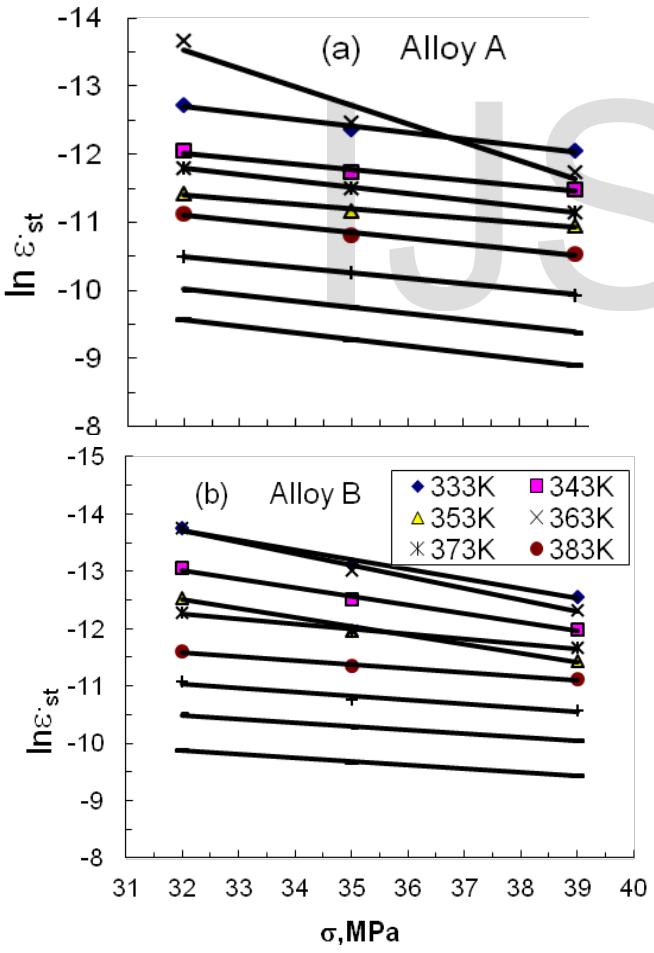

Fig.(3): (a, b) Relation between $\ln\dot{\varepsilon}_{st}$ and σ at different deformation temperatures, T, for alloy A and alloy B.

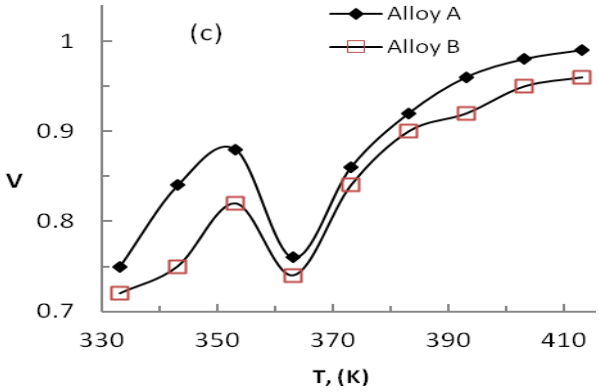

Fig.(3): (c) The dependence of the activation volume, V, on the working temperature, T, for both alloys A and B.

The activation volume, V, which denotes the volume over which the thermal energy is to concentrate in order to achieve the activation, using the relation [12].

$$V^* = kT(\Delta \ln \dot{\varepsilon} / \Delta\sigma) \qquad (3)$$

where k is Boltzmann's constant, V =∂ $\ln\dot{\varepsilon}_{st}$ /∂σ is derived from the slopes of the straight lines of Fig. 3 (a and b), the temperature dependence of V is given in Fig. 3c for both alloys A and B.

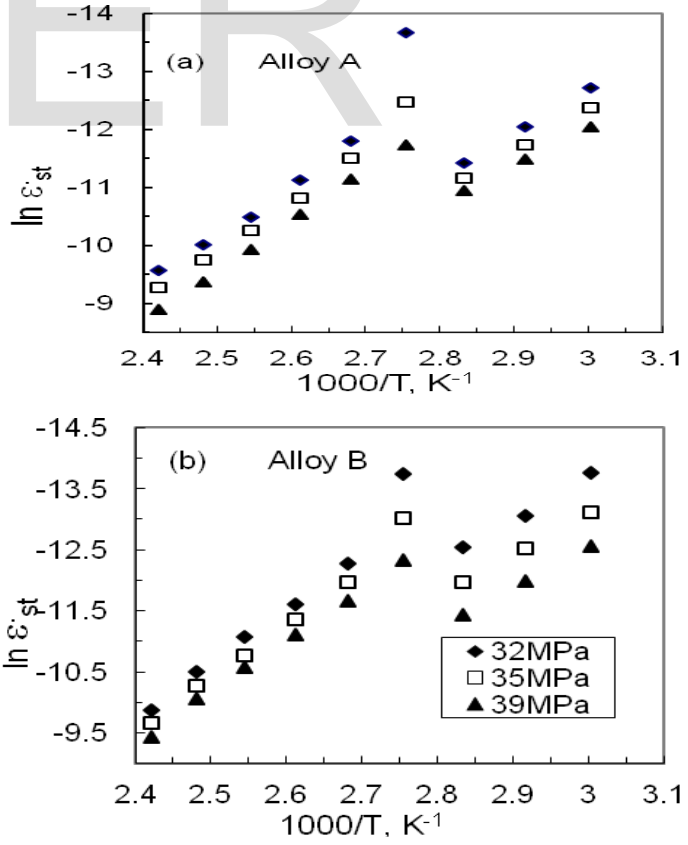

Fig. (4): Relation between ln ($\dot{\varepsilon}_{st}$) and (1000/T) K^{-1}, for different applied stresses for both alloys A and B.

The activation energy of the steady state creep, Q_{st}, for both alloys was calculated using an Arrhenius equation of the form [11].

$$\dot{\varepsilon}_{st} = A \exp(-Q_{st}/kT) \quad (4)$$

where T is the working temperature, A is constant.

The activation energies calculated from the slopes of the straight lines relating ln $\dot{\varepsilon}_{st}$ and (1000/T) K^{-1} given in Fig. 4 (a and b) for the applied stresses σ = 32, 35 and 39 MPa, show that two slopes can exist for each line depends on the applied temperature range.

The obtained average activation energies in the temperature range 333- 353 K (before transition) were 59.99 kJ/mole for alloy A and 66.16 kJ/mole for alloy B. While in the temperature ranging from 373 to 413K (after transition) the values were changed to 72.45 kJ/mole for alloy A, and 78.03 kJ/mole for alloy B.

The analysis of XRD patterns obtained for samples of both alloys A and B heat treated in the temperature range 333- 383 K (cooled to room temperature) revealed the presence of Sn matrix.

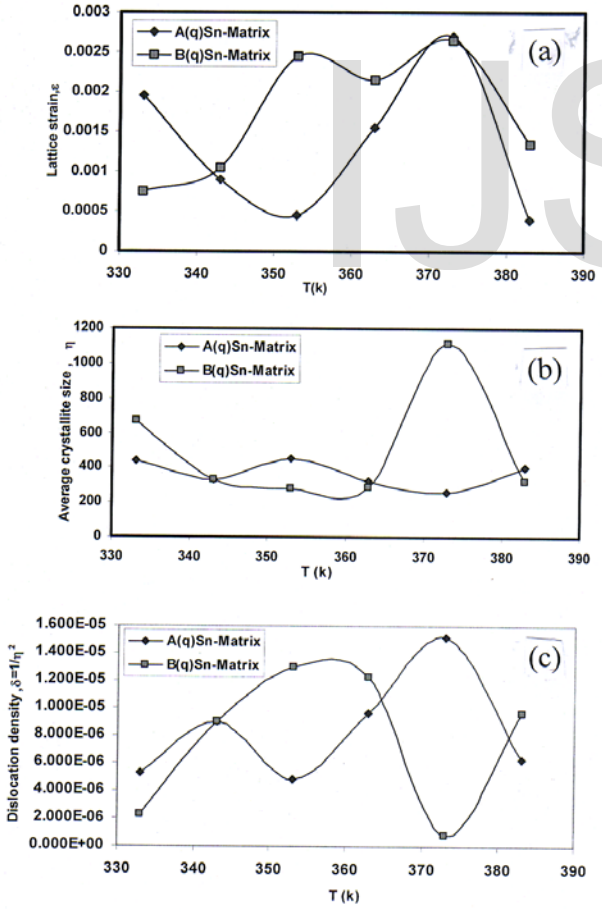

Fig.(5): Temperature dependence of (a) lattice strain,ε, (b) average crystallite size, η and (c) dislocation density, δ, for Sn planes to both alloys A and B

The temperature dependence of the average lattice strain ε_{av}, the average crystallite size, λ_{av}, and the dislocation density, δ, obtained for Sn planes in both alloys are given in Fig. 5 (a, b and c), respectively, together with the lattice constants (a) and its residual lattice strain $\Delta a/a$ in Fig. 6 (a and b) and its residual lattice strain $\Delta c/c$ in Fig. 7 (a and b).

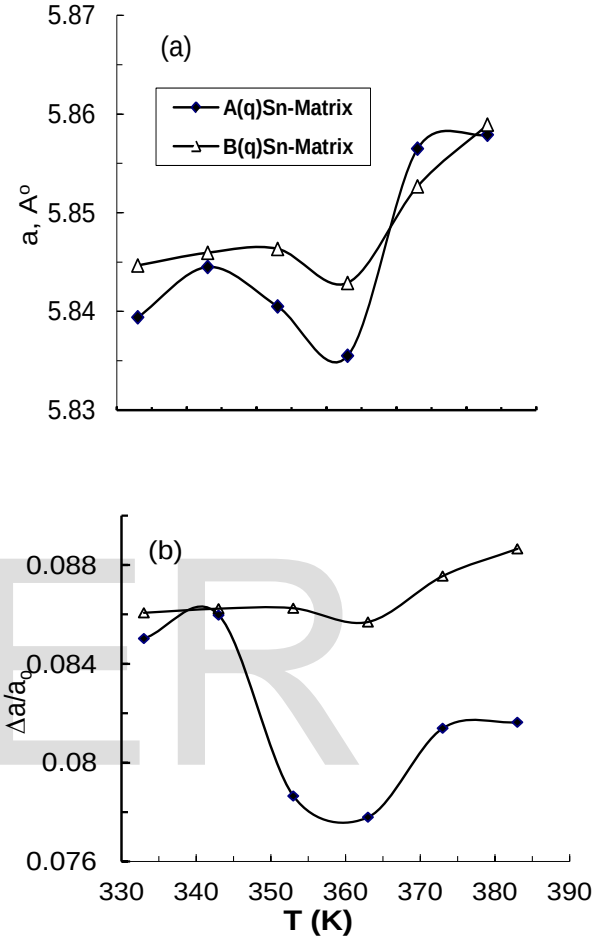

Fig. 6 (a, b): The effect of temperature on the lattice parameter (a) and the residual lattice strain $\Delta a/a_o$ for both alloys A and B.

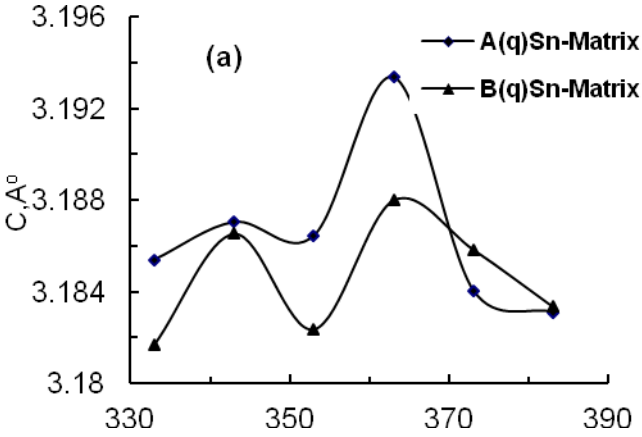

Fig.7: (a) The effect of temperature on the lattice parameter c,

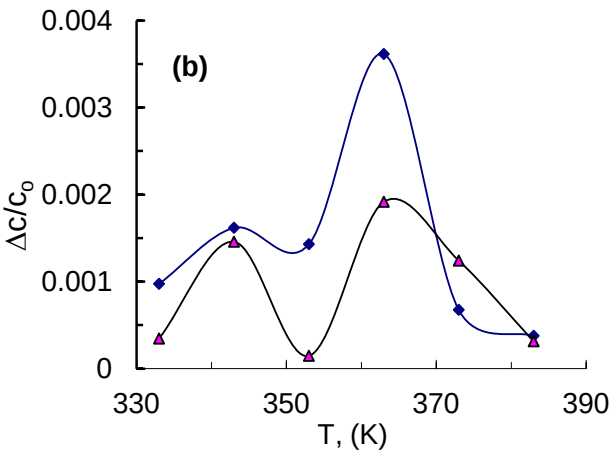

Fig.7: (b) The effect of temperature on the residual lattice strain, $\Delta c/c_o$.

4 DISCUSSION

The strength of binary alloy increases with the increase in second phase content or adding third alloying element which decrease the dislocation mobility. At certain temperature the thermally induced phases will generally be the same features whether they stem from a formation or a dissolution process. Hence, the controlling factor for strength of an alloy will be the existing amount of the phase and the nature of the medium surrounding the matrix [13].

The solute atoms distort the solvent lattice and change the average size of its elementary cell. The increased strengthening which results due to a decrease in lattice constant is stronger than that due to an increase in lattice constant. Accordingly, the strengthening due to Bi of radius (0.156 nm) in Sn (0.151 nm), will be smaller than Sb (0.145 nm) in Sn, which has small radius than Sn. This is clear in Fig. 1, where the tertiary samples are harder than the samples without Sb. Besides temperature and the applied stress which modify largely the effective forces in a material, the tensile properties still depend mainly on the type of the dispersed phase being coherent or incoherent with the matrix. These types differ in the mode of interaction with glide dislocations [14] of the existing dislocation system.

The increase of creep strain rate with increasing the aging temperature and applying the stress during creep observed in Fig. 1, might be the result of the dissolution of the coherent β-phase (GPZ) in the α-matrix and the increase in the homogeneity of the distribution of Bi atoms in the α-phase at higher temperatures [15].

The sequence of the curves becomes irregular in the transformation region. It appears that the alloy B has much higher creep resistance than the binary alloy A. It can also be seen that, the materials exhibit characteristics of the secondary creep immediately after loading with very little primary creep. It appears that the hardening of the matrix with the creep strain was recovered immediately because of the high temperature (> $0.5T_m$), which makes the hardening rate equal to the recovery rate right a way.

The peak values of the parameter $\dot{\varepsilon}_s$ Fig. 1 (a and b) observed at 353K might be due to structural variations taking place in the vicinity of this temperature [16]. It is seen that under the same test conditions alloy A yields creep rates higher than those of alloy B. This can be explained by dislocation motion across precipitates, which might be one of the important mechanisms under consideration and which could be affected in this temperature regime by the formation and dragging of a solute cloud [17].

On the basis of evidence and interpretation accepted in literature about Sn–Bi alloy, the present data in Fig. 1, establish as the fact that, distinct mechanisms of deformation are dominant at low and high levels of strain. Because of the absence of twinning in this alloy, the dominant low rate mechanism is the thermally activated grain boundary sliding (GBS) and the high rate slip mechanism[18].

The increased steady state creep rate with increasing temperature and/or stress in Fig. 1, indicates an easier motion of the existing dislocations caused by the external thermal or mechanical energy. The increase in the strain rate sensitivity parameter, m, with increasing temperature can be explained on the basis of dislocation mechanism [8]. In the low temperature range (333-353K) the alloy A has the highest strain rate sensitivity parameter, m, i.e., the highest creep resistance than the alloy B. In the high temperature range (363 - 413K) a reversed behaviour.

The increase in the activation volume by increasing temperature in Fig. 3c, can be explained on the basis of the dislocation density as the activation volume is directly proportional to the average spacing of dislocations [19]. Due increase in thermal energy, the dislocation density decreases and the average distance between dislocations increases. This indicates that alloy B is harder than alloy A, which implies that the dislocation density is higher in alloy B. Consequently, the average distance between dislocations decreases in alloy B than in alloy A. This leads to a decrease in the activation volume with

increasing temperature. This is in consistance with Fig. 3c, which shows that the level of the activation volume values is lower for alloy B.

The activation energy values in the low temperature range before transformation for both the creep stages in both the alloys, suggest that the creep process in this stage is controlled by grain boundary sliding or migration mechanisms. At elevated temperatures, suggest a gliding dislocation mechanism, thus the activation energies for the formation and migration of vacancy increase with order, resulting in higher activation energies for diffusion and creep, (78.03 kJ/mol) for alloy B compared to (72.45 kJ/mol) for alloy A , and therefore lower creep strain.

The analysis of X-ray diffraction patterns obtained for both the alloy samples, heat treated in the temperature range 333-383K then quenched to room temperature, revealed the presence of Sn matrix. Temperature dependence of both lattice strain ε, and dislocation density δ as $1/\eta^2$ are shown in Fig. 5 (a and c), which is contrary to the behaviour of the crystallite size η in Fig. 5b. It is clear that small crystallite size is due to large lattice strain and high dislocation density .The quenched state has small grains and increasing temperature increases grain size due to thermal strain recovery and a decrease of dislocation density. The fluctuations in the values of the crystallite size in Fig. 5b and the corresponding inverse variations of lattice strain and dislocation density depend mainly on the thermal variations in the different structural components of the alloy. The parameters ε, δ in Fig. 5 deduced from X-rays data confirms the behaviour of the activation volume in Fig. 3c, which is deduced from creep measurements.

For temperature below 353 K, α- phase (Sn -rich phase) and β-phase (Bi -rich phase) coarsen and the solubility of Bi in Sn increases with increasing the testing temperature until the transition temperature was observed at (353K) after which the β-phase dissolves completely [17, 19 - 21]. This increase in solubility leads to the formation of the β-phase (rich in Bi) + Sn-phase, this structure may cause the decrease in the lattice parameters, a and c. The residual strains, Δa/a, Δc/c values of these parameters at 353K are shown in Figs. (6b and 7b) and their contribute to the increasing softening has observed in the Fig.1, at higher temperatures. This softening may be attributed to the redistribution and coarsening of β-phase rich particles. It is observed that the tertiary alloy containing Sb behaves in the same way as the binary alloy at different temperatures but with different values as both Bi and Sb have the same surface activity nature [22].

In the temperature rang 353K - 363K, the parameter, Δa/a, decreased while the parameter related to c is increased. This shows that the crystal lattice shrunk in the basal plane and expanded in the c-direction with the formation of, α- phase (rich in Sn) +β-phase (Bi -rich phase).

A redistribution process of Bi and /or Sb solute atoms in the Sn matrix may take place, depending on the existing medium and the external factors such as temperature and stress, which may cause some of the solute atoms to be less activated at the quenching temperature and the low temperature, 363K, to reach their expected positions at the grain cores as states the surface activity theory [22]. Therefore, it is probable that some solute atoms will disperse near the Sn grain boundary regions and pin the mobile dislocations leading to this increased strength. It is clear that the strengthening due to Sb is higher than that of Bi as observed in Figs. (1, 2 and 3c).

For temperature above 363K, the parameter, Δa/a , increases, while the parameter, c, decreases with the formation of single β-phase (Sn -rich phase), due to the dissolution of β-rich particles and the homogenization in the alloy. This state leads to the rapid softening of the alloy samples with increasing temperature, Figs. 1, 3c and 6. This is clear from the observed behaviour of the temperature dependent dislocation density δ as $1/\eta^2$ in Fig. 5c, which is opposite to that of the behaviour of the crystallite size in Fig. 5b.

It is clear that the small crystallite size is due to large lattice strain and high dislocation density .The quenched state has small grains and increasing temperature increases grain size due to thermal strain recovery and a decrease of dislocation density. The fluctuations in the values of the crystallite size of Fig. 5b and the corresponding inverse variations of dislocation density in Fig. 5c depend mainly on the thermal and athermal variations in the different structural components of the alloy. The parameter in Fig. 5c, δ deduced from X-rays data confirms the behaviour of the activation volume in Fig. 3c, which is deduced from creep measurements.

5 Conclusion

The obtained creep curves exhibit the characteristics of the secondary creep results after loading with very little primary creep.

The variation in the creep parameter ε'_{st} with increasing testing temperature was explained on the basis of coarsening

and dissolution of β-phase (Bi-rich phase) occurring in Sn–Bi alloys.

The steady state strain rate sensitivity parameter (m), which indicates the level of creep resistance was found to be higher for alloy A than alloy B below the transition temperature 353K. The behaviour was reversed above 353K due to the high thermal effect on alloy A.

The activation energies obtained indicate two mechanisms; grain boundary sliding with partially diffusion before transition temperature region and the dominant mechanism which is the cross slipping mechanism after transition region.

REFERENCES

[1] F. Abd El-Salam, A.M. Abd El-Khalek, R.H. Nada, A. Fawzy. 2008 Mat. Characterization 59, 9 -17.

[2] "Material science and metallurgy", Herman W. P ollack, (Ruston publ. comp. Inc. 2nd.ed.1977)

[3] Alloy phase Diagrams; ASM Handbook: Vol.3, ASM International; materials park: OH; (1992) pp.1- 206.

[4] Morris, J. W.; Goldstein, J.L.F.; and Mei, Z; 1993 JOM; 45, 25- 57.

[5] K. Suganuma; Current opinion in Sol. Stat., and Mater. Sci., 5 (2001) 55-64.

[6] N. C. Lee, Soldering and Surface Mount Technology; 9 (1997) 64- 65.

.

[7] D. Miltin, C.H. Raedu, R.W. Messlar, 1999 J. Metall., Mater. Trans. A. Phys. Metall. Master, S.G.(USA), 30A,1, 115.

[8] B. A. Khalifa, M. R. Nagy, G. S. Al-Ganainy and R. Afify. 2006 Egypt. J. Solids, 29, 84.

[9] A. F. Abd El- Rehim, 2007 J. of alloys and compounds 440, 127-131.

[10] R.H. Nada, 2004 Physica B 349, 166.

[11] A.M. Abd El-Khalek, 2012 Materials Science and Technology 28, 1, 77.

[12] F. Abd El-Salam, R.H. Nada, A.M. Abd El- Khalek, N.R. Nagy, R. Abd El – Haseb, 2010 Mat. Sci. and Eng., 527, 2962- 2968.

[13] F. Abd El-Salam, M. M. Mostafa, L. A. Wahab, M. T. Mostafa, Sh. M. Abd El- Aziz, 2008 Mat. Sci. and Eng. A 478, 71- 76.

[14] C.C. Lee, R.W. Chuang, D.W. Kim, 2004 Mater. Sci. Eng., A 374, 280.

[15] M.M.Mostafa, R.H.Nada, F.Abd El-Salam, 1994 Phys. stat. sol.(a) A143, 297.

[16] M. Dragan et al. 2007 J. of Alloys and Compounds 438, 150.

[17] M. M. El- Sayed, F. Abd El-Salam and R. Abd El-Hasseb, 1995 Phys. stat. sol.(a) 101, 147, 401.

[18] Y.S. Kim, K.S. Kim, C.W. Hwang, K. Suganuma, 2003 J. of Alloys and Compounds 352, 237–245.

[19] M.A. Mahmoud, G. Graiss, 2002 Journal of Materials Science 37, 2215-2223.

[20] M.W. Thompson, (Defects and Radiation Damage in Metals), Cambridge University press (1969) pp.76 - 80.

[21] R.S. Sundar, T.R.G. Kutty, D.H. Sastry, 2000 Intermetallics, 8, 427- 437.

[22] V.K. Semencheno (Surface Phenomena in Metals and Alloys), Pergamon, London (1961) pp. 129.